Advanced Frame Element for Seismic Analysis of Masonry Structures: Model Formulation and Validation

Eva Raka, Enrico Spacone*†, Vincenzo Sepe and Guido Camata

Department of Engineering and Geology, University "G. D'Annunzio" of Chieti Pescara,
viale Pindaro 42, I-65127 Pescara, Italy

ABSTRACT

This paper presents a masonry panel model for the nonlinear static and dynamic analysis of masonry buildings suitable for the seismic assessment of new and existing structures. The model is based on an equivalent frame idealization of the structure and stems from previous research on force-based frame elements. The element formulation considers axial, bending and shear deformations within the framework of the Timoshenko beam theory. A phenomenological cyclic section law that accounts for the shear panel response is coupled, through equilibrium between shear and bending forces along the element, with a fiber-section model, that accounts for the axial and bending responses. The proposed panel model traces with a low computational burden and numerical stability the main aspects of the structural behavior of masonry panels and is suitable for analyses of multi-floor buildings with a relatively regular distribution of openings and with walls and floors organized to grant a box-like behavior under seismic loads. The model capabilities are validated though analyses of simple unreinforced masonry panels and comparisons with published experimental results. The model accuracy is strongly dependent on the fiber and shear constitutive laws used. However, the formulation is general and laws different from those employed in this study are easily introduced without affecting the model formulation.

KEY WORDS: Masonry structures; nonlinear analyses; equivalent frame; fibre elements; force-based formulation; cyclic analysis.

1. INTRODUCTION

Unreinforced masonry (URM) buildings, often conceived to carry vertical loads only, are found all over the world and represent the main part of the historic heritage in Italy and in several other countries worldwide. Many of them have shown poor performance in past earthquakes, due to the masonry intrinsic heterogeneity and its low tensile and shear strengths, which in turn stem

*Correspondence to: Enrico Spacone, Department of Engineering and Geology, University of Chieti Pescara, viale Pindaro 42, I-65129 Pescara - Italy

† E-mail: espacone@unich.it

from the low mechanical properties of the masonry constitutive materials. Simple mechanics-based reliable models are needed for assessing the seismic performance of a large number of masonry buildings in seismic prone areas, such as the South Mediterranean countries. This research area has become increasingly significant in recent years due to the frequent occurrence of natural earthquakes [e.g. in Italy: Umbria-Marche, 1997; Molise, 2002; Salò, 2004; L'Aquila, 2009, Emilia Romagna, 2012] and the need to evaluate the seismic safety of large stocks of masonry buildings. Two main collapse mechanisms may be observed in masonry structures after an earthquake: in-plane and out-of-plane mechanisms [1-4]. Extensive damage surveys carried out by the authors in several historical centers after the L'Aquila 2009 earthquake [5] show that the parameter with the highest influence on the strength of existing masonry buildings is the effectiveness of the connections between horizontal and vertical load resisting elements. When the connections between orthogonal walls, or between walls and floor slabs or between walls and roof are poor, the building cannot behave as a box and the seismic vulnerability mainly depends on the out-of-plane collapse mechanisms of the resisting macroelements (e.g. masonry walls or portions of them), rather than on the in-plane excessive stress state in the masonry. Without a box-like behavior, collapse of masonry buildings can occur at low to moderate ground shaking intensities [6].

To assess the seismic safety of buildings with box-like behavior, where in plane failure of the vertical walls is of interest, nonlinear equivalent frame models, rather than more sophisticated and computationally more demanding bi- and tri-dimensional finite elements, are often used both in research and practice. This paper proposes an equivalent frame element for masonry walls that can efficiently model the in-plane seismic behavior of masonry panels for nonlinear static and dynamic analyses of panels, walls and buildings.

2. FRAME-EQUIVALENT MODELING OF MASONRY STRUCTURES

Because of its brittle behavior and often irregular constitutive pattern, unreinforced masonry is a difficult material to model. The development of simple yet computationally efficient and reliable procedures capable of solving complex nonlinear analyses for the seismic design and assessment of masonry structures is thus a challenging task. A reliable structural model includes different parameters such as the structure geometry and the masonry properties, the latter being difficult to represent because of the high anisotropy and nonlinearity of the material. At the same time, the model should require an acceptable computational effort and simplicity in the determination of the input parameters. Three-dimensional finite element analyses are still too lengthy and complex to be applicable to a large number of nonlinear static or dynamic analyses because of: numerical stability, computational time cost, identification of large number of numerical parameters, availability of reliable constitutive laws. For the above reasons, the equivalent frame modeling of masonry buildings - where the masonry walls are represented by one-dimensional macro-elements (or frame elements) - is a valid alternative largely used in research and practice.

Several researchers from seismic prone southern European countries have recently proposed and used simplified methodologies based on the equivalent frame approach. A general description of different models for frame-type and macroelement modeling is reported by Magenes [7] and more recently by Marques and Lourenço [8]. The first models were developed in the 70's (see POR method [9]) and were based on simplified elasto-plastic shear force-inter story drift laws. More recently, the equivalent frame approach was used to develop nonlinear programs for masonry structures, such as TREMURI [10] or SAM [11]. In these programs, nonlinear frame elements (or macro-elements) are formulated for the wall components. Macro-element models offer the major advantage of being accurate in describing the main failure models of masonry walls (bending and shear) while retaining acceptable computational times. They obviously present some limitations as well, namely due to the inaccurate simulation of the structure geometry, the connection between macro-elements (spandrels are connected with the piers at a point, while in reality there is a more complex stress transfer mechanism between horizontal and vertical elements that takes place over the node) and the need to derive generalized bending and shear constitutive laws. Also, spandrels and panels are often modeled using the same constitutive laws, but the spandrels' shear behavior is more brittle, since the axial compression is almost zero. To overcome these limitations modified two-dimensional macro-elements were proposed by Vanin and Foraboschi [12] using strut and tie models and by Caliò et al. [13] using nonlinear springs. The latter is implemented in the computer code 3DMacro [14]. Recently, Casolo and Peña [15] have developed a specific rigid element approach for the in-plane dynamic analysis of masonry walls.

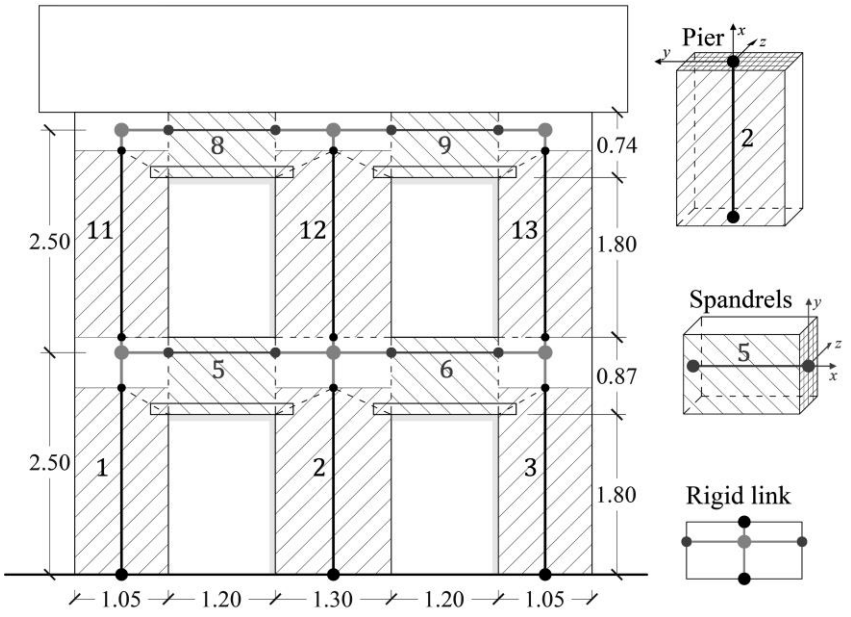

Figure 1. Equivalent frame discretization of a wall.

In equivalent frame models, the wall deformation is assumed to be lumped in the piers and spandrels, while the other wall components are assumed rigid. A typical frame equivalent model is shown in Figure 1, where the piers and the spandrels are represented by columns and beams, respectively. In the example of Figure 1 the pier height is determined according to Dolce [16]: the pier is higher than the opening to approximately account for the nodal deformation, while the spandrels' width is assumed equal to the openings' width.

The main advantage of this numerical approach is its computational efficiency, which makes it suitable for nonlinear analyses of large building stocks, including building aggregates in historical centers. With an appropriate formulation, the macroelement model can reasonably approximate the cyclic shear and flexural response of masonry walls. More specifically, the main failure mechanisms of masonry piers subjected to horizontal (e.g. seismic) loads [17] are:

a) rocking (flexural) failure: failure is related to pier crushing in the compressed zone;

b) shear-diagonal failure: pier failure is due to excessive shear stresses and the formation of inclined diagonal cracks;

c) shear-sliding failure: failure is associated to horizontal cracks in the bed-joints.

The rocking failure, associated with the flexural behavior of the pier, is typically assessed starting from the assumption that plane sections remain plane and computing the maximum compressive stress at the wall base. In elements made of brittle, unreinforced materials such as URM piers, bending is highly dependent on the compression force in the pier. If the masonry material is assumed to have zero tensile strength and no axial compression is applied to the pier, the pier has zero theoretical bending strength.

The shear failure of URM piers associated with diagonal cracking is the result of several interacting factors that are difficult to describe and simulate. Based on tests performed in Ljubljana (Slovenia) on URM piers with fixed-fixed boundary conditions, Turnšek and Čačovič [18] proposed the formulation used in this study to estimate the shear strength of URM piers: diagonal shear failure is reached when the principal tensile stress at the pier center reaches a critical value, defined as the masonry reference tensile strength. The resulting shear strength expression is:

$$V_d = \frac{f_{tu}\, lt}{b}\sqrt{1+\frac{\sigma_0}{f_{tu}}} \tag{1}$$

where f_{tu} is the masonry tensile strength, σ_0 the section average compression stress ($\sigma_0=N/lt$), l and t the width and the thickness of the wall section, respectively, and b a parameter that depends on the pier aspect ratio and varies within a range of 1.0 to 1.5 and is constant outside these bounds [19]. The above formula is general, more specific expressions exist for brick masonry [20].

The sliding-shear strength is also evaluated on the basis of approximate formulas. For example, Eurocode 6 [21] uses the following expression:

$$V_s = f_{vd}\, l_c\, t = \left(\tau_0 + 0.4\sigma_n\right)\cdot l_c\, t \tag{2}$$

where f_{vd} is the design shear strength, l_c is the length of the compressed portion of the section and σ_d is the average compression stress on the section ($\sigma_n=N/l_c t$). The masonry panel shear strength is the minimum between Eqs. (1) and (2). More details on the in plane behavior of masonry walls are found in [22] and [23].

A pier fails in shear or in bending according to the weaker of the two mechanisms. The two mechanisms are related through equilibrium and a correct representation of the wall behavior should account for this equilibrium.

3. PROPOSED APPLICATION OF A FORCE-BASED MODEL

This paper proposes the extension of an existing distributed plasticity, force-based frame element - that was originally developed for reinforced concrete frames [24-25] – to the description of the in-plane behavior of URM walls. Though the original element is available in several research programs, its implementation in the open source computational platform OpenSees [26] is used in this work because of the software flexibility and ease of implementation of new features. The element formulation is based on the Timoshenko beam theory and assumes that plane sections remain plane. The element behavior is obtained by numerical integration of the nonlinear response at the monitored sections along the element. The model uses the Gauss-Lobatto integration scheme in which two integration points coincide with the element end sections, where bending failure is expected to take place. Figure 2 shows the general cross section discretization into n_z by n_y fibers of area A_f. This discretization accounts for the axial and flexure behaviors, and automatically accounts for their interaction. In this paper, only uniaxial bending is considered, though all figures refer to the general biaxial bending case, since the formulation is identical. Nonlinear cyclic uniaxial stress-strain laws σ–ε are used for all fibers. For example, the nonlinear material constitutive law shown in Figure 2 takes into account the softening branch of the masonry behavior. Masonry (bricks plus mortar) is modeled as a homogeneous continuum. Thus the quasi-brittle uniaxial constitutive law used should be able to yield, through the fiber section discretization, the overall compression-tension and bending responses of a wall.

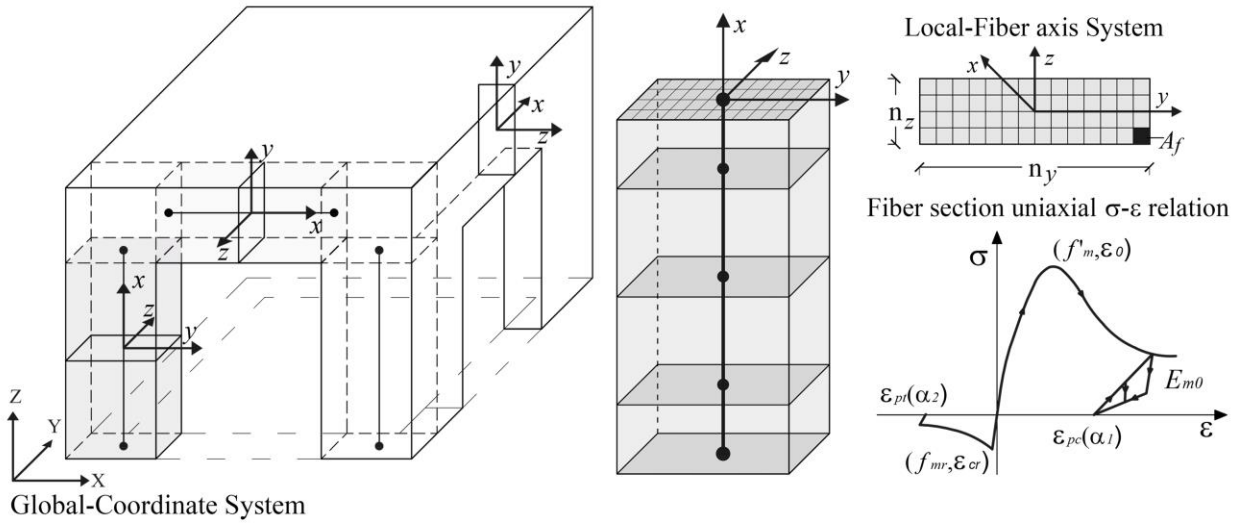

Figure 2. Forced-based, fiber-section elements (for masonry piers and spandrels) in the 3D global system;distribution of Gauss-Lobatto points, section subdivision into fibers and fiber nonlinear stress-strain law.

Different behaviors can be expected based on the type of masonry wall (i.e. URM walls made of rubble stones, walls made of regular stones, walls made of hollow or solid bricks, walls made of concrete bricks, types of mortar, etc.), thus material parameters need to be calibrated from tests [27-29] or from code-specified mechanical properties. The proposed masonry frame model also accounts for the shear deformation and failure mode. Shear, axial and bending are described within the framework of the Timoshenko beam theory. The element formulation is based on the work developed by Marini and Spacone [30]. At the section level, bending and axial responses are decoupled from the shear response. The section forces and the corresponding deformations are:

$$\mathbf{S}(x) = \left[M(x) \quad N(x) \quad V(x) \right]^T \tag{3}$$

$$\mathbf{e}(x) = \left[\kappa(x) \quad \varepsilon_0(x) \quad \gamma(x) \right]^T \tag{4}$$

Force-based elements stem from the weak form of compatibility, expressed through the Principle of Virtual Forces, which in the case of the beam takes the form:

$$\delta \, \mathbf{P}^T \mathbf{U} = \int_0^L \delta \, \mathbf{S}^T(x) \, \mathbf{e}(x) dx \tag{5}$$

where **P** and **U** denote the element nodal forces and displacements, respectively. The section bending moment and axial force are obtained by adding the contributions of the single fibers. The shear response is modeled via a phenomenological cyclic nonlinear *V*-γconstitutive law. The expressions for section forces **S**(*x*) and section tangent stiffness matrix **k**(*x*) are:

$$\mathbf{S}(x) = \begin{bmatrix} -\sum_{fiber=1}^{nfib} \sigma_{fiber} A_{fiber} y_{fiber} \\ \sum_{fiber=1}^{nfib} \sigma_{fiber} A_{fiber} \\ V = V(\gamma) \end{bmatrix} \tag{6}$$

$$\mathbf{k}(x) = \begin{bmatrix} \sum_{fiber=1}^{nfib} E_{fiber} A_{fiber} y_{fiber}^2 & -\sum_{fiber=1}^{nfib} E_{fiber} A_{fiber} y_{fiber} & 0 \\ -\sum_{fiber=1}^{nfib} E_{fiber} A_{fiber} y_{fiber} & \sum_{fiber=1}^{nfib} E_{fiber} A_{fiber} & 0 \\ 0 & 0 & dV / d\gamma \end{bmatrix} \tag{7}$$

where *nfib* is the number of section fibers, σ_{fiber} is the fiber stress, E_{fiber} is the fiber tangent modulus, A_{fiber} is the fiber area, y_{fiber} is the distance from the fiber centroid to the section reference axis *z* (in the case of simple bending). The section model is schematically shown in Figure 3.

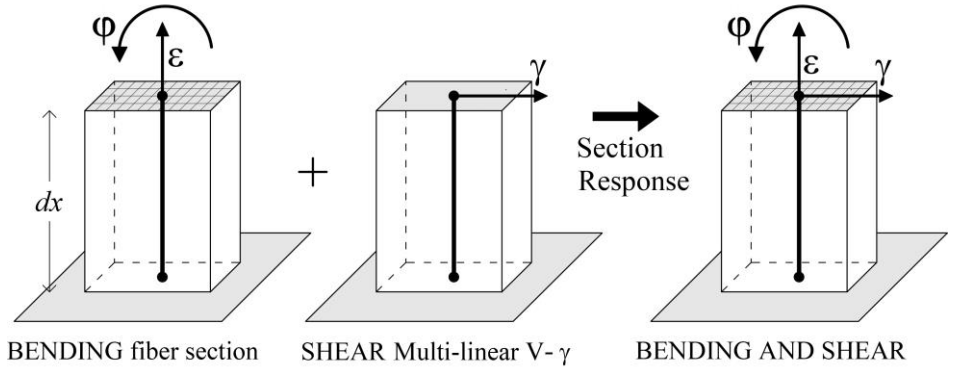

Figure 3. Schematic section wall formulation.

Two constitutive laws, borrowed from the OpenSees one-dimensional material library, are used to simulate the masonry uniaxial behavior, one with and the other without tensile strength. Both laws, originally developed for concrete, lend themselves to model the uniaxial response of masonry, since they are both quasi-brittle materials. The first law used is the Kent and Park model [31] modified by Scott et al. [32] (Figure 4a). De Santis and De Felice [33] used the same law and calibrated the material parameters from experimental evidence on historic brick walls samples tested in compression. Similarly, the material parameters used in this work were verified against the results of the tests on URM brick walls carried out by other authors [34-35]. Within the equivalent frame approach, a force-based approach has been recently proposed by Addessi et al. [36], but they use a phenomenological law for the bending response and the applications are

limited to monotonic loading. Addessi et al. [36] provide a comprehensive description of the element formulation, including rigid end offsets use for the rigid links of Figure 1.

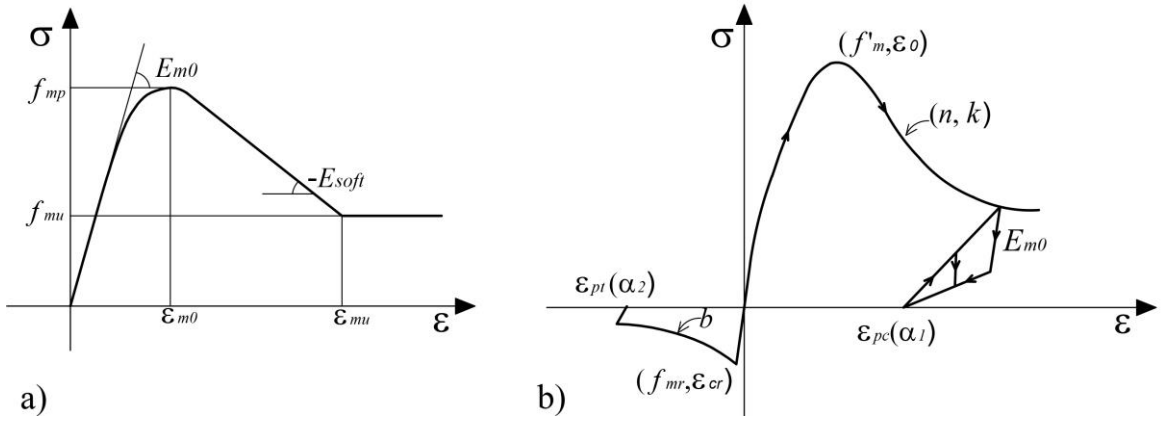

Figure 4. Uniaxial constitutive laws used for the masonry fiber
a) Modified Kent and Park [32] b) Orakcal et al. [37].

The second law was proposed by Orakcal et al. [37] and is shown in Figure 4b. This law considers the material tensile strength and thus offers a more accurate description of the masonry behavior. The compression behavior is based on the work by Thorenfeldt et al. [38]. The compression envelope curve is described by the following equation:

$$\sigma_m = f_m^{'} \frac{n\left(\frac{\varepsilon_m}{\varepsilon_0}\right)}{n-1+\left(\frac{\varepsilon_m}{\varepsilon_0}\right)^{nk}} \tag{8}$$

where f'_m is the masonry compressive strength, ε_0 is the strain at peak compressive stress, n is the compressive shape factor and k is the post-peak compressive shape factor. Suggested values for n and k are found in Orakcal et al. [37]. The tensile behavior is based on the work by Belarbi and Hsu [39], where the tensile curve response is divided in the two following branches:

$$\varepsilon_m \le \varepsilon_{cr} \Rightarrow \sigma_m = \left(\frac{f_{mr}}{\varepsilon_{cr}}\right)\varepsilon_m \tag{9}$$

$$\varepsilon_m > \varepsilon_{cr} \Rightarrow \sigma_m = f_{mr}\left(\frac{\varepsilon_{cr}}{\varepsilon_c}\right)^b \tag{10}$$

where f_{mr} is the tensile strength, ε_{cr} is the strain corresponding to the tensile strength peak and b is a constant input parameter borrowed from Belarbi and Hsu [39] and described in Orakcal et al. [37]. Other constitutive laws have also been used by the authors to describe the masonry uniaxial response, including elastic and elastic-perfectly plastic responses, as discussed in the examples of section 4.

The phenomenological shear force-deformation (V-γ) behavior follows the nonlinear constitutive law proposed by Lowes et al. [40] and is shown in Figure 5a. The definition and calibration of this model require 16 parameters for the response of the negative and positive response envelope curves: $V_{1p,}$ $V_{2p,}$ $V_{3p,}$ $V_{4p,}$ define the force points on the positive response envelope, $\gamma_{1p,}\gamma_{2p,}\gamma_{3p,}\gamma_{4p}$ define the corresponding deformation points. V_{1n}, V_{2n}, V_{3n}, V_{4n} define the force points on the negative response envelope, $\gamma_{1n,}$ $\gamma_{2n,}$ $\gamma_{3n,}$ γ_{4n} define the corresponding deformation. Additional parameters define the unloading-reloading paths, as described in Lowes et al. [40].

For calibrating the material parameters of the loading envelope indicated in Figure 5a, following Magenes & Calvi [17] and Tomaževič [41], the initial diagonal cracking shear V_{1p} was assumed equal to 90% of the ultimate shear strength V_{3p}. The value of the shear deformation at the end of the initial elastic branch (γ_{1p}) is computed as V_u/K_{Vel}, where $K_{Vel}=GA_s$ is the wall initial elastic shear stiffness. Alternatively, γ_{1p} can be estimated following FEMA 356 [45], that suggests a conventional drift range 0.075-0.1%. Numerical simulations by the authors show that the value of the initial elastic stiffness does not significantly affect the results. In the present work, the intermediate point 2 is placed for simplicity halfway between points 1 and 3. Based on work by Magenes & Calvi [17] and pseudo-dynamic tests carried out at the ELSA Laboratory [42] it was found that the ultimate drift γ_{3p} (corresponding to the attainment of the wall shear capacity) can be approximately set to 0.4%. This is also the value indicated in NTC 2008 [43]. The drift limit γ_{4p} is set equal to 1.0%, as proposed in FEMA 356 [45]. A discussion on the calibration of the post peak behavior can be found in FEMA 306 [44]. Finally, V_{4p} - the residual shear strength– is conventionally set equal to a percentage of V_{3p} (the default value in the present work is V_{4p} = 20% V_{3p}). Additional information on the mechanical shear response parameters' selection can be found in Penna et al. [48]. In the cyclic analyses presented in this work, all parameters in the negative branch are set equal to the parameters in the positive branch. The above parameters' values can be refined based on additional in depth studies and experimental data relevant to the URM type under consideration.

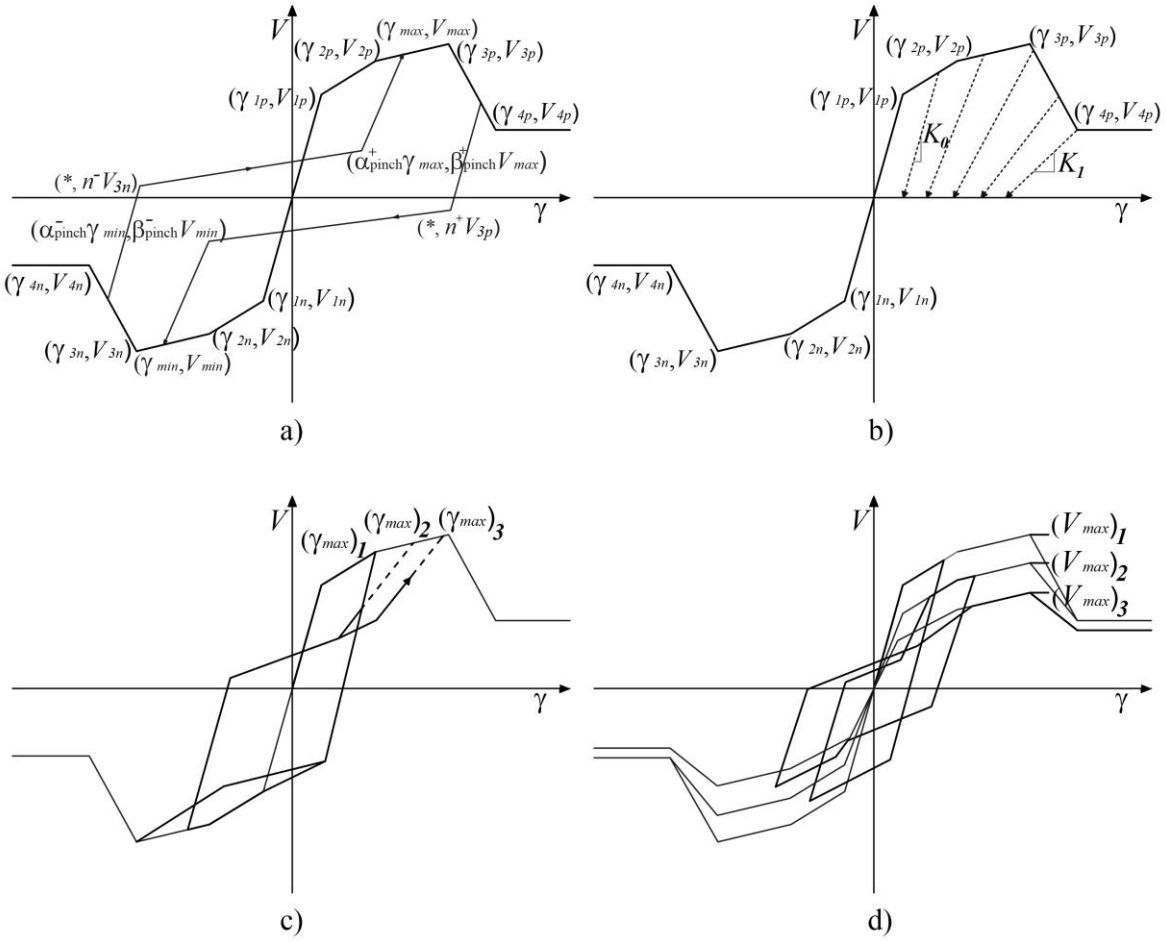

Figure 5. Shear phenomenological constitutive law (adapted from [40]):
a) loading and reloading envelopes; b) unloading stiffness degradation;
c) reloading stiffness degradation; d) strength degradation.

Hysteretic damage is simulated through deterioration in the unloading stiffness (Figure 5b), deterioration in the reloading stiffness (Figure 5c), and strength deterioration (Figure 5d). Lowes et al. [40] provide details on the deterioration rules, which they propose as a more general version of the damage index by Park and Ang [46]. Penna et al. [48] present an interesting discussion on cyclic damage that can be useful in selecting damage parameters. Experimental data, if available, should help calibrate the law for the specific case under consideration. In the present work, the default values for the parameters governing the deterioration rules suggested by Lowes et al. [40] were used.

In the proposed frame element for masonry walls, the fiber section discretization accounts for the axial and bending responses, while the shear response is described by the above phenomenological law. There is no interaction at the section level between shear and axial-bending behaviors, however equilibrium at the element level enforces equilibrium between bending and shear forces. As shown in Marini [30], the element flexibility is the sum of the shear and bending flexibilities. Additionally, when shear failure takes place the bending moment cannot increase, and vice-versa, because of equilibrium between bending and shear forces at the

element level. The element formulation is however general enough to allow, in future developments, the implementation of a more general section formulation that accounts for *N-M-V* interaction. This approach has already been pursued for reinforced concrete elements (Petrangeli et al. [47], Tortolini et al. [49]), but it is at this stage deemed too complex and potentially unstable for an unreinforced material such as URM walls. As previously discussed, in this work the wall shear strength is the minimum between diagonal and base sliding failure. In all cases considered, shear failure was attributed to diagonal shear failure.

4. MODEL VALIDATION

In order to validate its precision, the proposed model is applied to different URM panels of increasing complexity. First of all, the bending model based on the fiber-section approach is compared with an existing model widely used in research. Pushover analyses are then performed on a masonry panel to determine the drifts at which failure occurs and to compare the results with formulations available in literature. The validation of the model is extended to walls with different geometries and subjected to monotonic and dynamic loadings. Finally the model results are compared to published experimental results.

4.1 Axial-flexural behavior: fiber section analysis

The capability of the proposed fiber section model to describe the axial-flexural response of a masonry wall section is assessed by comparing a section response with that obtained following the closed-form equations presented in Penna et al. [48]. Because the results are given in terms of rotations and displacements (rather than section generalized deformations), the full wall of Figure 6 is considered. The wall cross section dimensions are t=0.6m, l=3m and the height is h=2m.

The complete mechanical properties of the panel are shown in Table I, where G is the shear modulus, E the compressive Young modulus, ρ the masonry specific weight, f_m the masonry compressive strength, f_{tu} the masonry tensile strength and μ the friction coefficient.

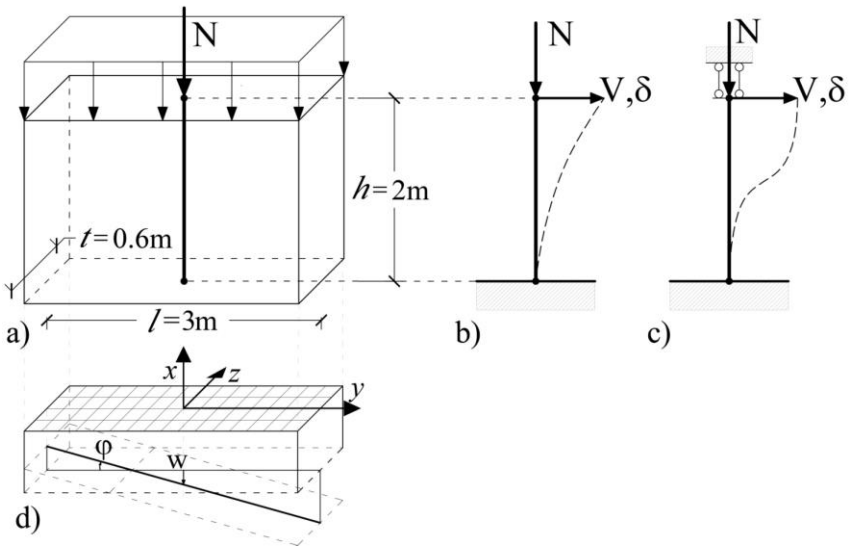

Figure 6. Details of sample wall:a) geometry and loading conditions; b) cantilever configuration boundary conditions; c) fixed-fixed configuration boundary conditions; d)fiber section deformed configuration.

Table I. Mechanical properties

G[MPa]	E[MPa]	ρ[kN/m3]	f_m[MPa]	f_{tu}[MPa]	μ[-]
230	870	19	1	0.1	0.4

Figure 7 shows the three uniaxial masonry constitutive laws with no tension used to model the panel: elastic, elastic-perfectly plastic and modified Kent and Park model.

The pushover analysis is performed with a fixed vertical loads N=500kN and imposed horizontal displacements at the wall top, as shown in Figure 6.

Figure 8 shows the φ - w interaction curves obtained using the three constitutive laws in Figure 7, where – following the notation by Penna et al. [48] - φ denotes the rotation of the top section of the wall and w its total vertical displacement (see Figure 6d). In the initial step of the pushover analysis the whole cross section is compressed. The figure shows that for small rotations, before the section cracks, the behavior of the wall with elastic and elastic-perfectly plastic material is almost identical, while the two responses depart for increasing rotations. The vertical displacement at zero rotation is different for the nonlinear material because the Kent and Park constitutive law is nonlinear from the onset of loading.

Figure 9 compares the results obtained using the proposed fiber model with those obtained with the formulation by Penna et al. [48]. Following Penna et al. [48], the analysis is performed with the elastic perfectly-plastic masonry constitutive law shown in Figure 7 and Figure 9 indicates a very good agreement between results with the two formulations.

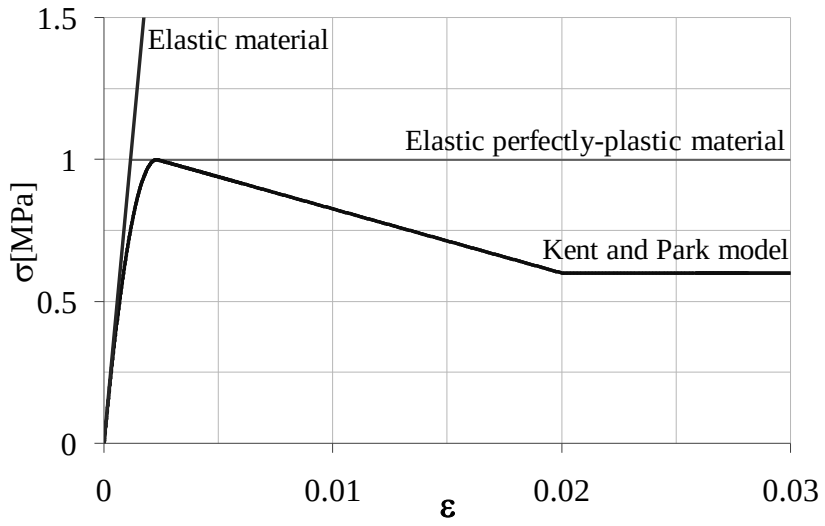

Figure 7. Masonry constitutive laws used to analyze the panel of Figure 6b.

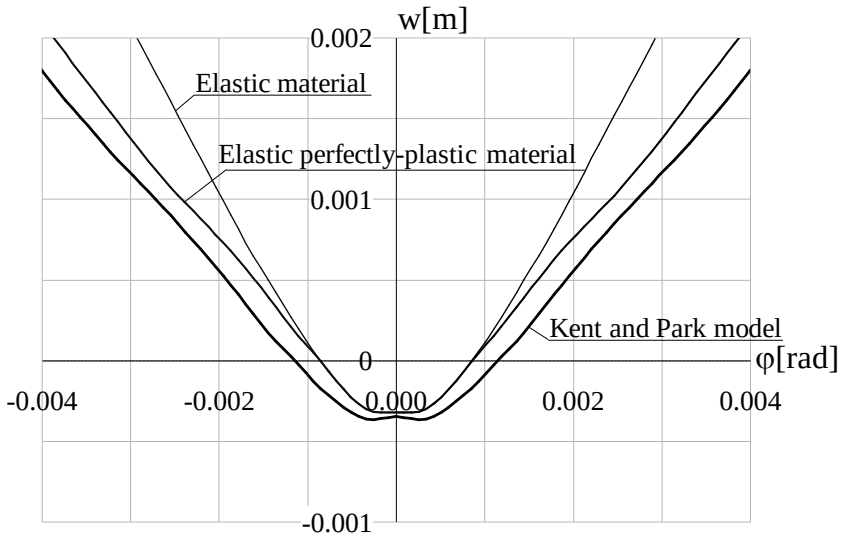

Figure 8. Interaction between vertical displacement and rotation φ-w (analysis case shown Figure 6b).

Figure 10 compares the section M-N interaction diagram obtained with the two formulations and shows good agreement between the proposed fiber-section formulation and the closed-form solution by Penna et al. [48]. It is important to point out that while the closed-form solution by Penna et al. [48] requires pre-assigned masonry laws (elastic-perfectly plastic in this case), the fiber section formulation can use any kind of constitutive law, with and without tension response, monotonic or cyclic, without any change in its formulation or implementation.

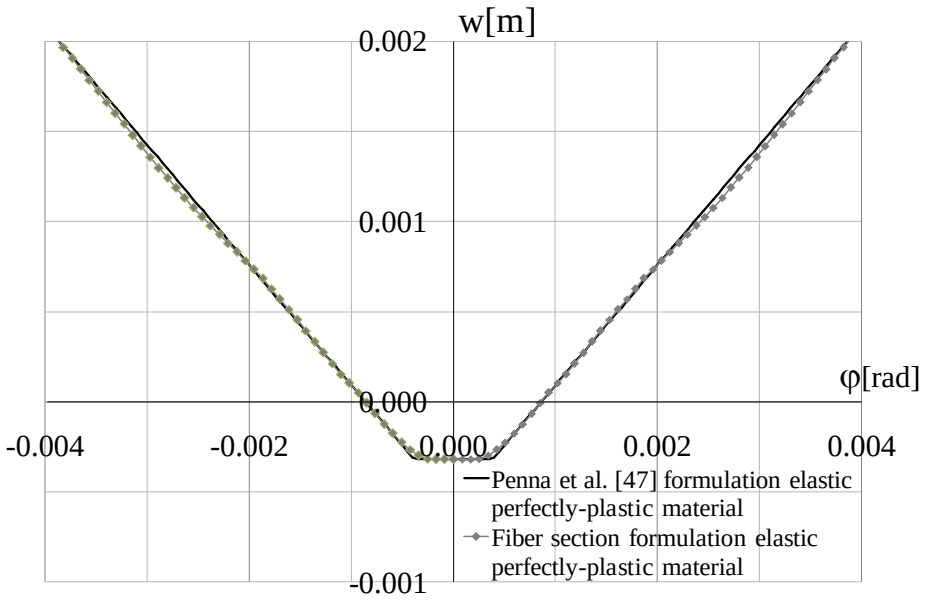

Figure 9. Interaction between vertical displacement and rotation: comparison between fiber section model and Penna et al. [48] formulation in the case of elastic-perfecty plastic material (analysis case shown Figure 6b).

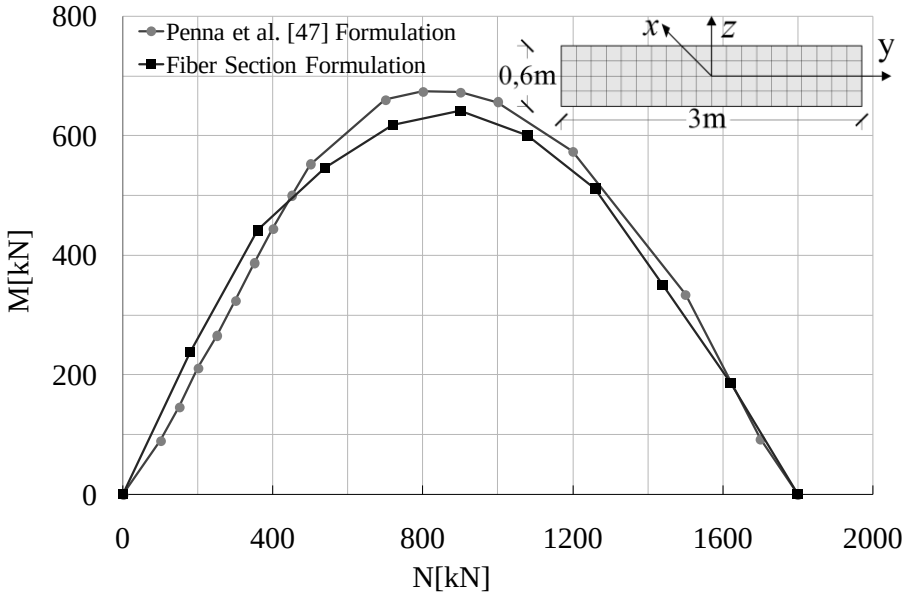

Figure 10. M-N Interaction diagram: Comparison between fiber section model and results from theory by Penna et al. [48].

4.2 Pushover analysis of a simple wall with combined shear and flexural behavior

The wall of Figure 6 is used here to show the interaction between axial-bending and shear responses. The wall is analyzed using different axial load ratios. Fixed-fixed boundary conditions

are introduced and the modified Kent and Park model ([31] and [32]) with no tensile strength is used to describe the uniaxial response of the masonry material.

The analyses are first performed with axial load N=180kN (N = 0.1Nmax, where N_{max} is the wall strength under pure compression) with and without the shear behavior.

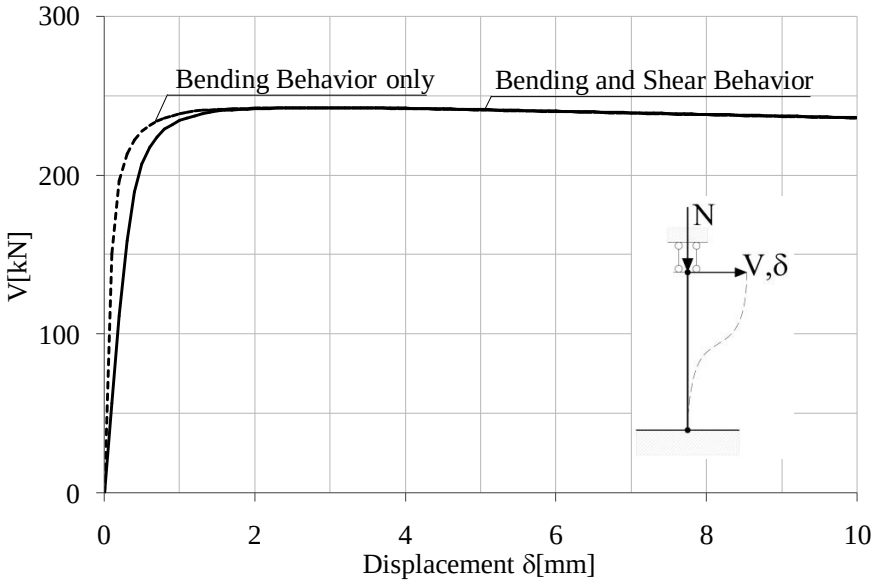

Figure 11. V-δ base shear displacement curve for N=180kN (N = $0.1N_{max}$ for loading case of Figure 6c).

The shear strength due to diagonal cracking is computed according to eq.(1) using the following parameters: f_{tu}=0.1MPa; l=3000mm; t=600mm; b=1.0; σ_0=N/lt=0.1MPa. Thus $V_d = f_{tu}\, lt/b\sqrt{1+\sigma_0/f_{tu}} = 254\,\text{kN}$ .The shear response follows the nonlinear shear constitutive law shown in Figure 12 (reported for two axial compression levels), which is obtained using appropriate parameters for the law shown in Figure 5.

For an axial load N = $0.1N_{max}$, the maximum base shear corresponding to flexural failure (i.e. provided by the fiber model) is 242kN, and is thus lower than the shear capacity of the panel. The wall failure for this case of low axial load is due to flexural failure. The results of Figure 11 indicate that for this level of axial load the addition of the shear behavior does not change the failure mode but increases the wall flexibility on the initial pseudo-elastic branch due to the additional shear flexibility.

For a higher vertical axial load N, the flexural strength increases and shear failure becomes the governing failure mode. For instance, in the case of N=225kN (i.e. N = $0.125N_{max}$), the wall shear capacity due to diagonal cracking calculated from eq.(1) is V_d= 270kN. Figure 12 shows the nonlinear V-γ shear constitutive law used in the analyses. The base shear curves with and without shear deformation are shown in Figure 13. The maximum base shear corresponding to the flexural capacity obtained with the fiber section analyses is V_f=298kN.

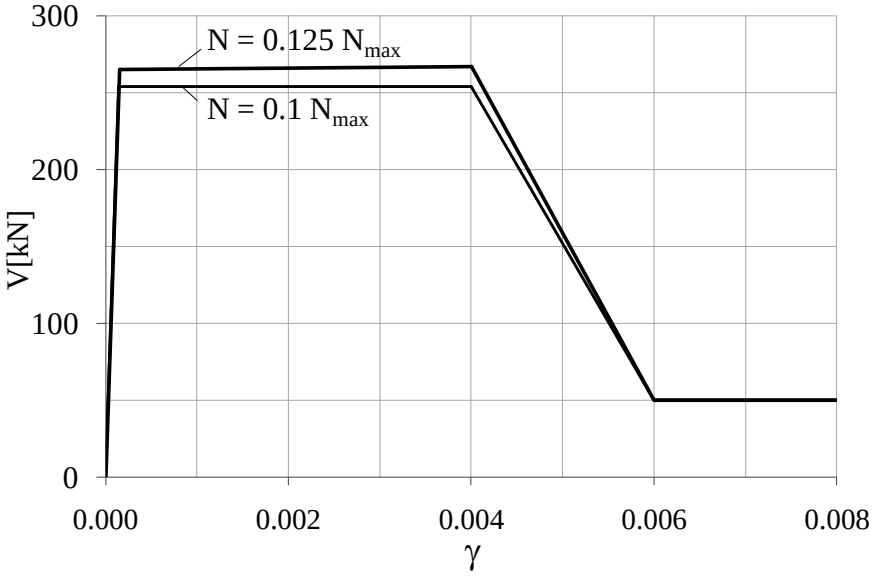

Figure 12. V-γ shear response (for N = 0.1N_{max} and N = 0.125 N_{max}).

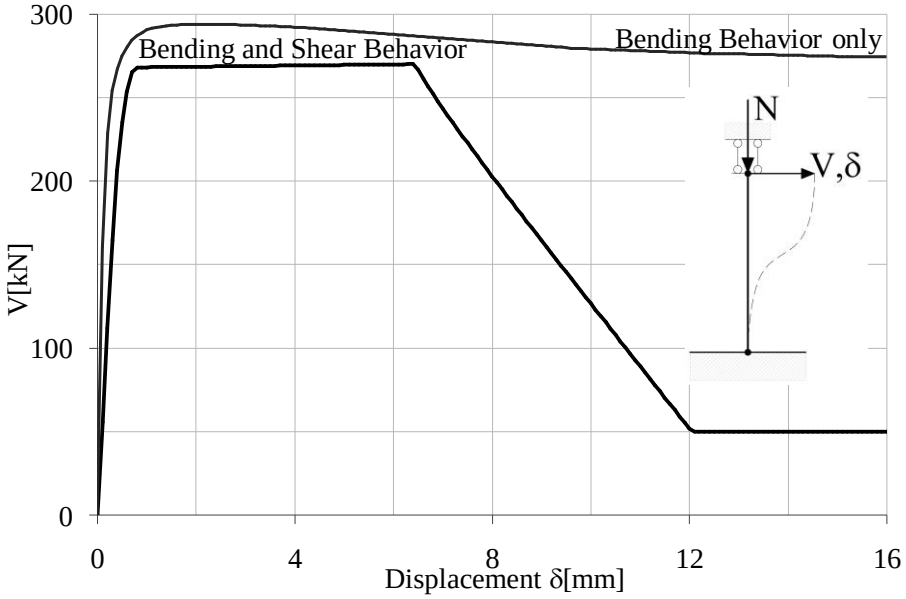

Figure 13. V-δ base shear displacement curve for N = 0.125N_{max}.

In the ascending branch, the wall response is stiffer when the shear deformation is not accounted for, as already seen in the previous case. When the shear behavior is introduced, the wall fails due to shear failure, as correctly shown in Figure 13.

The interaction between flexure and shear behavior is easily shown in Figure 14, which plots, for the given wall, the base shear corresponding to flexure and diagonal shear failure of the wall. For small axial load, the wall flexural capacity is lower than the shear capacity. As the applied axial load is increased, the flexural capacity increases at a higher rate than the shear

capacity, thus for an axial load equal to approximately $0.11N_{max}$ diagonal shear failure, as computed from eq. (1), governs the wall response. This behavior is correctly described by the proposed model.

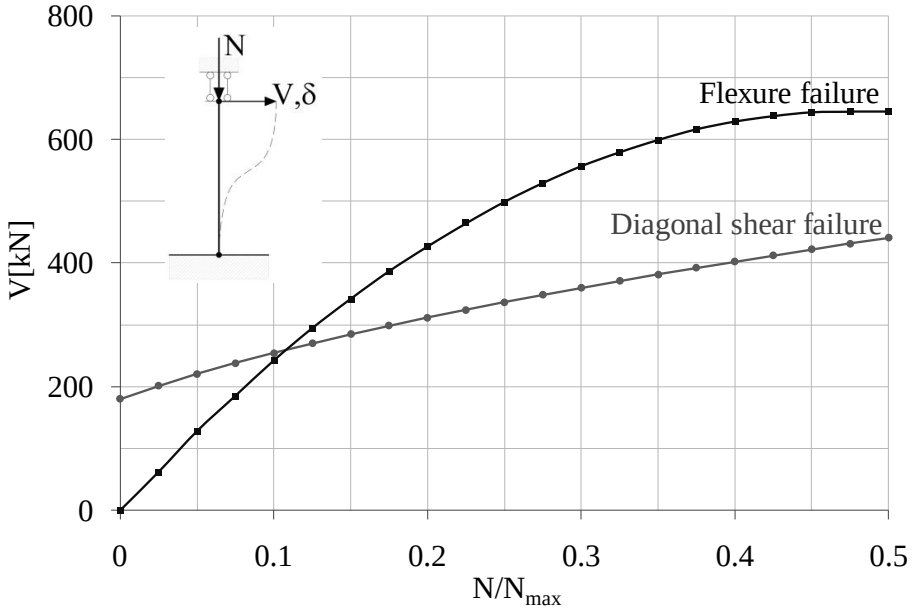

Figure 14. The V-N Interaction diagram.

4.3 Correlation with experimental results

Next, the proposed application of the frame model to masonry structures is validated through correlation analyses with available experimental results. The first test analyzed was carried out by Abrams and Shah [29]. They tested a single wall under monotonic loading: the wall is fixed at the base and the vertical and horizontal loads are applied at the top of the wall as shown in Figure 15. A summary of the specimen properties is given in Table II. The material properties were selected to reflect the structural characteristics of a typical older masonry wall in North America [29].

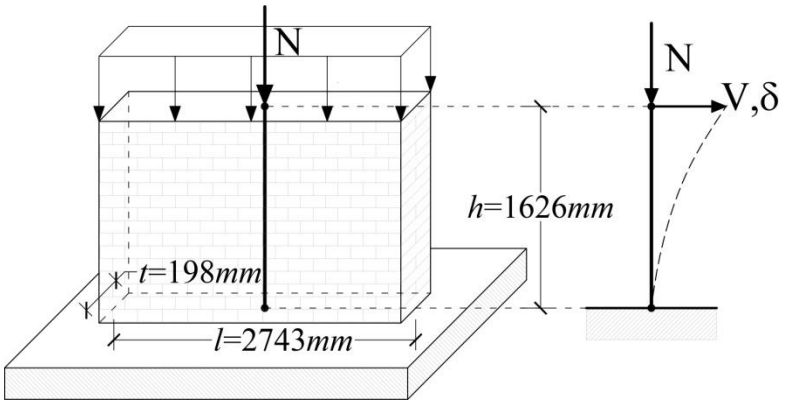

Figure 15. Geometry of the panel tested by Abrams and Shah [29].

Table II. Mechanical properties reported in Abrams and Shah [29]

Specimen	Length [mm]	Height [mm]	Thickness [mm]	E [MPa]	G [MPa]	f_m [MPa]	f_{tu} [MPa]
W2	2743	1626	198	2460	1130	6.28	0.15

The wall was subjected to a low vertical axial load of N=282kN, equivalent to a vertical stress of 0.32MPa. The diagonal shear capacity (V_{3p}) is computed from eq. (1) and is equal to 175kN. The shear response is represented by the nonlinear law proposed by Lowes et al. [40] as shown in Figure 5. The other parameters are calculated as described in Section 3 and summarized in Table III. Given the low axial load, the first crack to develop was in flexure at the base. At higher lateral displacement, a diagonal crack formed initiating failure. A good agreement is found between the numerical and experimental results, in particular in terms of the wall lateral shear capacity (Figure 16). The numerical test was repeated with three different values of the initial elastic shear stiffness K_{Vel}. The best fit results from the use of $K_{Vel} = GA_s$ Even though the authors suggest using the above value for the elastic shear stiffness, using half or twice $K_{Vel} = GA_s$ does not result into a significant difference in the response.

Table III. The mechanical parameters of the phenomenological shear model (Figure 5)

V_{1p},	V_{2p}	V_{3p},	V_{4p}	γ_{1p},	γ_{2p}	γ_{3p}	γ_{4p}
157.5	174.9	175	120	0.00035	0.00075	0.004	0.01

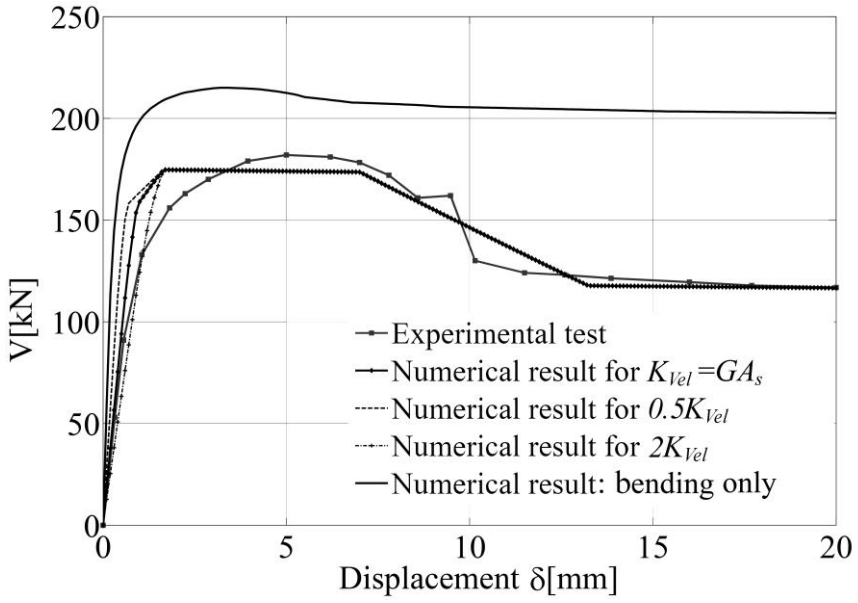

Figure 16. V-δ base shear displacement curve for panel of Figure 15

Next, the experimental research on masonry panels carried out by Anthoine et al. [42] at ELSA (European Laboratory for Structural Assessment, Ispra, Italy) is considered. Anthoine et al. [42] investigated the influence of slenderness on the masonry walls behavior in quasi-static cyclic conditions up to failure by testing walls with the same mechanical properties but with different height/width ratios. The brick size was 250x120x55mm and hydraulic lime mortar was used to build the masonry panel.

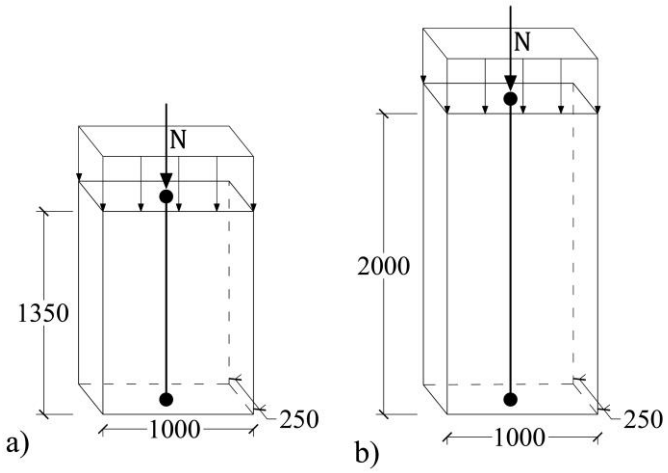

Figure 17. Geometry of panels tested by Anthoine et al., [42]:
a) squat wall b); slender wall. All dimensions are in mm.

Several walls were tested under controlled boundary conditions, with fixed base and fixed rotation at the panel top. In the two tests considered in this study, the vertical load N was kept constant and equal to N=150kN, that is $N \approx 0.1N_{max}$.The two panels have the same section dimensions (width l=1000mm and thickness t=250mm) but different heights; the squat wall (Figure 17.a) height is h=1350mm and the slender wall (Figure 17.b) height is h=2000mm.

The constitutive law proposed by Orakcal et al. [37] was used in the analyses to describe the masonry bending behavior. The main material properties used are summarized in Table IV. The first four are reported in Anthoine et al. [42], while the remaining five are set to the default values indicated by [26]. The numerical simulations were performed with the same loading and boundary conditions of the experiments reported in [42]. The resulting uniaxial constitutive law used in the analyses is shown in Figure 18.

Table IV.Mechanical properties for the constitutive law by Orakcal et al.[37] and shown in Figure 4b

f'_m[MPa]	ε_0[-]	f_{mr}[MPa]	ε_{cr}[-]	n[-]	k[-]	b[-]	α_1[-]	α_2[-]
6.2	0.0009	0.18	1.8 E 10^{-5}	2	1	4	0.32	0.08

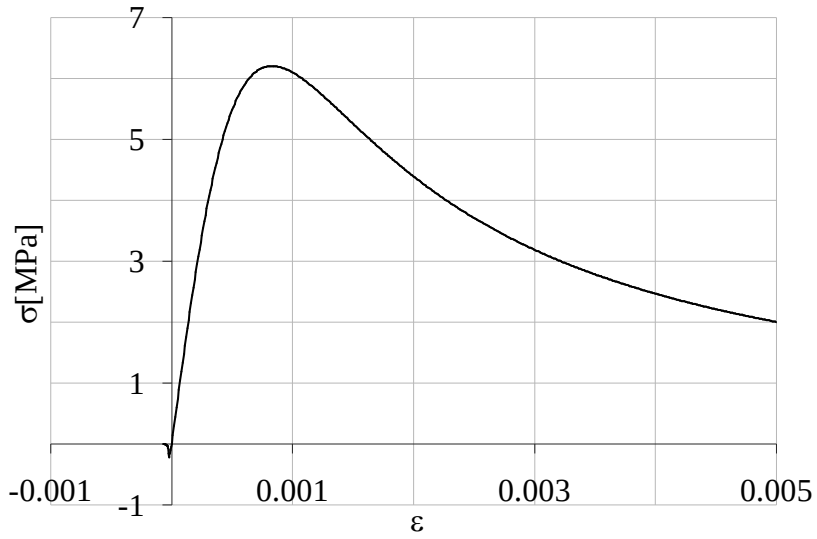

Figure 18. Uniaxial strain-stress constitutive law used for masonry.

The shear response is represented by the nonlinear shear law proposed by Lowes et al. [40] and described in Sect. 3. For a constant vertical axial load N=150kN (i.e. $0.1N_{max}$) the maximum diagonal cracking shear is calculated from eq. (1) and is equal to 86.3kN. The deformation at peak shear strength is γ=0.0008 (approximately computed dividing the shear strength by the shear elastic stiffness). The negative post-peak slope reflects the experimentally observed post-peak strength degradation. A single frame element was used to model each wall.

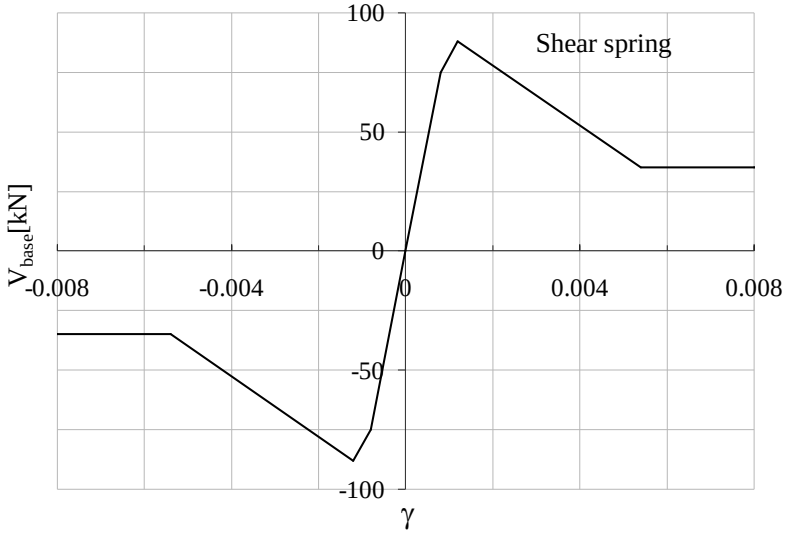

Figure 19. Shear model for the panels in Figure 17.

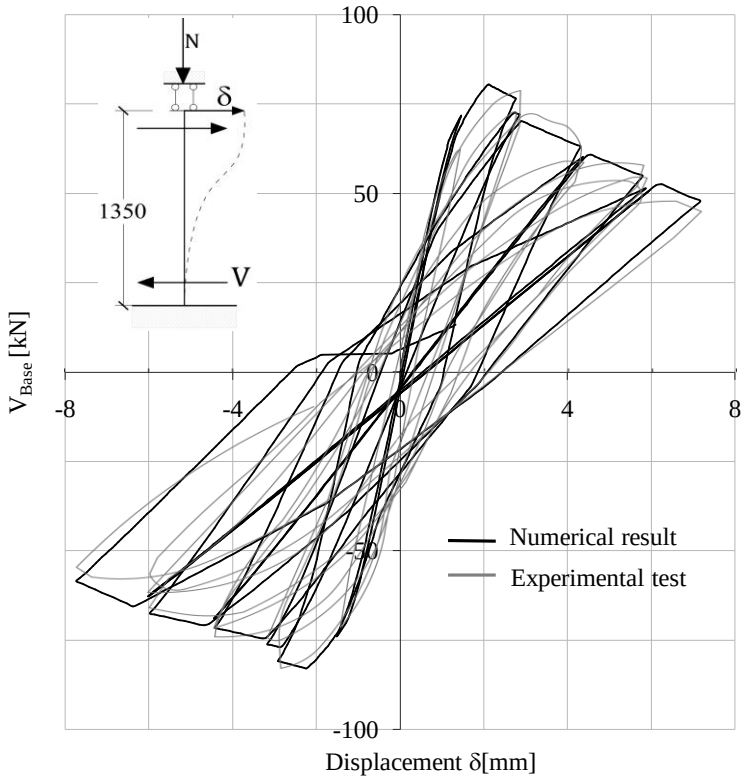

Figure 20. V-δ response curves of the squat wall: experimental (Antoine et al [42]) vs. numerical results.

In the experimental tests by Anthoine et al. [42], horizontal displacements of increasing amplitude were imposed to the panels' tops with three repetitions for each cycle. For the two walls of Figure 17, Figure 20 and Figure 21 compare the numerical predictions obtained with the proposed model with the experimental results by Anthoine et al. [42]. It is observed that the numerical analyses capture well the experimental results in terms of stiffness, strength and failure mode and are capable of simulating the cyclic behavior in terms of energy dissipation, strength degradation, stiffness degradation and pinching behavior.

More precisely, for the squat wall (Figure 20) the proposed model correctly reproduces the shear failure of the experimental test, dominated by shear diagonal cracking, and the post-peak response characterized by progressive stiffness degradation with significant loss of strength and hysteretic energy dissipation. For the flexure dominated slender wall, Figure 21 shows that the fiber model is capable of describing quite well the cyclic flexural behavior. The prevailing mechanism is flexural with a slight rocking. During cyclic loading the panel strength is reached quite rapidly but no significant loss of strength is caused by the cycles. There is little hysteretic energy dissipation and the unloading-reloading branches show the classical shape of the flexural response of unreinforced brittle materials due to crack closing on one side of the section and then opening on the other side.

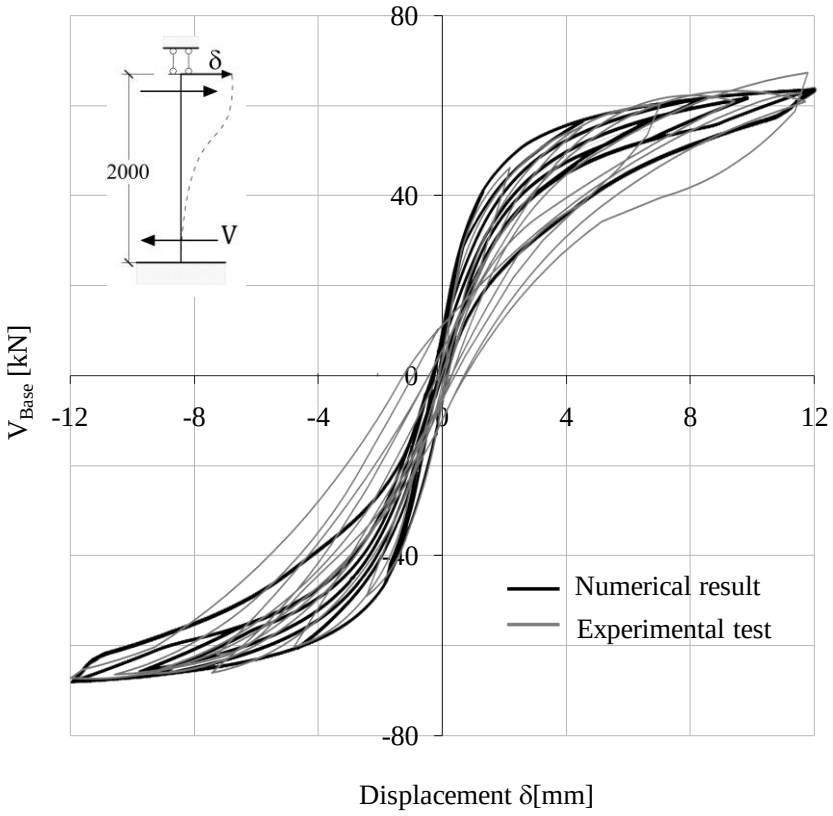

Figure 21. V-δ responses of the slender wall: experimental (Antoine et al [42]) vs. numerical results.

5. **CONCLUSIONS**

This work presents a model for describing the nonlinear monotonic and cyclic response of masonry structures applicable in the widely used equivalent frame approach. The proposed masonry frame element is capable of describing both the flexural and the shear response of masonry walls up to failure. The axial and flexural behaviors are obtained from a fiber-section model of the panel cross section, while the shear response is described through a phenomenological shear force-shear deformation law. The fiber section model automatically accounts for the influence of the axial compression on the flexural response of the wall. Bending and shear forces are in equilibrium during the analyses, thus the wall flexibility is the sum of the flexural and shear flexibilities, while strength is governed by the weaker of the two resisting mechanisms. This behavior is illustrated through simple panel tests and through comparisons with available experimental tests. These tests show that the element is capable of describing the salient characteristics of the response of masonry walls and report satisfactory comparison with experimental results. Accuracy of the predicted response is highly dependent on the material constitutive laws used, more so for the panel shear response. The phenomenological shear law strength values may be obtained from design code equations or derived from more sophisticated approaches. The element stability and computational efficiency were also tested. The element is fast and stability is typically guaranteed for the beneficial effect of the axial compression on the wall. Since the element formulation is “exact” within the Timoshenko beam theory assumptions,

one frame element is used for each flexible structural member. The study was also extended to the analysis of multi story walls and complete buildings: these analyses are the focus of future publications.

The proposed model can be effectively used for the nonlinear seismic analysis of single panels, multi-bay multi-story walls and three dimensional masonry structures that show a box behavior thanks to good connections between orthogonal walls and between walls and floors. The model is easily extendable to biaxial response of panels and walls, thus allowing the out of plane response of walls to be accounted for. Studies are also under way to extend the equivalent frame approach, and thus the use of the proposed model, to walls that show irregular openings and thus require care in the definition of the wall, spandrel and rigid zone geometry. Though the model described in this paper refers to unreinforced masonry, its extension to reinforced masonry is straightforward. The proposed model, similarly to currently available macro-models such as that by Penna et al. [48], can be effectively used in both research and practice to study and assess the nonlinear behavior of masonry structures.

ACKNOWLEDGEMENTS

Partial financial support from the ReLUIS program of the Italian Civil Protection Agency is acknowledged. The authors would also like to thank Prof. Luigi Sorrentino of the Sapienza University of Rome for giving his highly qualified feedback on the first author's PhD research.

REFERENCES

1. Giuffrè A. *Safety and conservation of historical centers: the Ortigia case*. Laterza ed.: Bari, Italy, 1993 [in Italian].
2. Doglioni F, Moretti A, Petrini V. *The churches and the earthquake.- From the vulnerabilities found in the Friuli earthquake to earthquake-proof improvement in the restoration, to a policy of prevention*. Lint Press: Trieste, Italy, 1994 [in Italian].
3. Petrini V, Casolo S, Doglioni F. Models for vulnerability analysis of monuments and strengthening criteria. *XI European Conference on Earthquake Engineering*, Paris, France, 1998; 179–198.
4. D'Ayala D, Speranza E. Definition of collapse mechanisms and seismic vulnerability of historic masonry buildings. *Earthquake Spectra* 2003; **19**(3): 479–509 DOI: 10.1193/1.1599896 .
5. Sepe V, Spacone E, Verazzo C. Impact of the L'Aquila 2009 earthquake on the small village of Poggio Picenze: Damage Assessment and Reconstruction Planning, *COST Action C26 Conference*, Naples, Italy, 2010; 1031-1036.
6. Tomaževič M, Weiss P, Velechovsky T. The influence of rigidity of floors on the seismic behaviour of old stone-masonry buildings. *European Earthquake Engineering* 1991; **5**(3): 28-41.
7. Magenes G, Braggio C, Bolognini D. *Simplified Methods for the Nonlinear Seismic Analysis of Masonry Buildings*. *CNR-GNDT*: Roma, 2001 [in Italian].
8. Marques R, Lourenço PB. Possibilities and comparison of structural component models for the seismic assessment of modern unreinforced masonry buildings. *Computers and Structures* 2011; **89**(21): 2079-2091.
9. Tomaževič M. *The computer program POR.* Report ZRMK, Ljubljana, 1978 [in Slovenian].
10. Lagomarsino S, Penna A, Galasco A, Cattari S. TREMURI program: an equivalent frame model for the nonlinear seismic analysis of masonry buildings. *Engineering Structures* 2013, **56**:1787–1799.

11. Magenes G, Della Fontana A. Simplified nonlinear seismic analysis of masonry buildings. *Proceedings of the British Masonry Society* 1998; **8**:190–195.
12. Vanin A, Foraboschi P. Modelling of masonry panels by truss analogy–Part 1. *Masonry Int*. 2009; **22**(1): 1-10.
13. Caliò I, Marletta M, Pantò B. A new discrete element model for the evaluation of the seismic behaviour of unreinforced masonry buildings. *Engineering Structures* 2012; **40**:327–338.
14. 3DMacro. http://www.murature.com/3DMacro/download.php [8 September 2014]
15. Casolo S, Peña F. Rigid element model for in-plane dynamics of masonry walls considering hysteretic behaviour and damage. *Earthquake Engineering and Structural Dynamics* 2007; **36**(8): 1029–1048.
16. Dolce M. Schematization and modelling of masonry buildings subjected to seismic actions. *L'Industria delle Costruzioni* 1991; **242**: 44–57 [in Italian].
17. Magenes G, Calvi GM. In-plane seismic response of brick masonry walls. *Earthquake Engineering and Structural Dynamics* 1997; **26**(11):1091–1112.
18. Turnšek V, Čačovič F. Some experimental results on the strength of brick masonry walls. *Proceedings of the 2nd International Brick & Block Masonry Conference*, Stoke-on-Trent, United Kingdom, 1970; 149–156.
19. Tomaževič M. Masonry Structures in Seismic Areas - A state of art Report. *9th European Conference on Earthquake Engineering*, Moscow, 1990; vol. A, 247-302.
20. Mann W, Muller H. Failure of shear stressed. *Proceedings of British Ceramic Society* 1980; **27**: 223-235.
21. Eurocode 6. *Design of masonry structures - Part 1-1: Common rules for reinforced and unreinforced masonry structures* (EN 1996-1-1) CEN, Comité Européen de Normalisation: Brussels, 2004.
22. Magenes G, Calvi GM. *Cyclic behaviour of brick masonry walls. Proceedings of the 10th World Conference on Earthquake Engineering*, Madrid, Spain, 1992; 3517–3522.
23. Turnšek V, Sheppard P. The shear and flexural resistance of masonry walls. *Proc. of the Intern. Research Conference on Earthquake Engineering*, Skopje, Macedonia, 1980; 517-573.
24. Spacone E, Filippou FC, Taucer FF. Fibre beam-column model for nonlinear analysis of R/C frames: part I. Formulation. *Earthquake Engineering and Structural Dynamics* 1996; **25**(7):711–725.
25. Spacone E, Filippou FC, Taucer FF. Fibre beam-column model for nonlinear analysis of R/C frames: part II. Applications. *Earthquake Engineering and Structural Dynamics* 1996; **25**(7):727–742.
26. OpenSees. http://opensees.berkeley.edu/OpenSees/user/download.php [14 September 2014]
27. Milosevic J, Lopes M, Gago AS, Bento R. Testing and modeling the diagonal tension strength of rubble stone masonry panels. *Engineering Structures* 2013; **52**: 581–591 doi: 10.1016/j.engstruct.2013.03.019.
28. Abrams DP. Strength and behavior of unreinforced masonry elements. *Proceedings of the 10th World Conference on Earthquake Engineering*, Madrid, Spain,1992; **6**: 3475-3480.
29. Abrams DP, Shah N. Cyclic load testing of unreinforced masonry walls. *Report No. 92-26-10*, Advanced Construction Technology Center—University of Illinois, Urbana, 1992.
30. Marini A, Spacone E. Analysis of Reinforced Concrete Elements Including Shear Effects, Structural Journal ACI 2006; **103**(5): 646-655.
31. Kent DC, Park R. Flexural members with confined concrete. Journal of the Structural Division ASCE 1971; **97**(7): 1969–1990.
32. Scott BD, Park R, Priestley MJN. Stress–strain behavior of concrete confined by overlapping hoops at

low and high strain rates. *ACI Journal Proceedings* 1982; **79**(1): 13–27.
33. De Santis S, de Felice G. A fibre beam-based approach for the evaluation of the seismic capacity of masonry arches. *Earthquake Engineering and Structural Dynamics* 2014; **43**(11): 1661–1681 doi: 10.1002/eqe.2416.
34. Lourenço PB. Computational strategies for masonry structures, PhD Dissertation. Delft University: Netherlands, 1996.
35. Binda L, Fontana A, Frigerio G. Mechanical behaviour of brick masonries derived from unit and mortar characteristics. *Proceedings of the Eighth International Brick and Block Masonry Conference, Dublin*, Ireland, 1988; **1**:205-216.
36. Addessi D, Mastandrea A, Sacco E. An equilibrated macro-element for nonlinear analysis of masonry structures, Engineering Structures 2014; **70**: 82-93 doi:10.1016/j.engstruct.2014.03.034.
37. Orakcal K, Massone LM, Wallace JW. Analytical modeling of reinforced concrete walls for predicting flexural and coupled-shear-flexural responses. *PEER-2006/07*, Pacific Earthquake Engineering Research Center, University of California, Berkeley, 2006.
38. Thorenfeldt E, Tomaszewicz A, Jensen JJ. Mechanical properties of high strength concrete and application to design. *Proceedings of the symposium: Utilization of high strength concrete*, Stavanger, Norway, 1987; 149-159.
39. Belarbi H, Hsu TCC. Constitutive Laws of Concrete in Tension and Reinforcing Bars Stiffened by Concrete. *ACI Structural Journal* 1994; **91**(4): 465-474.
40. Lowes LN, Mitra N, Altoontash A. A Beam-Column Joint Model for Simulating the Earthquake Response of Reinforced Concrete Frames. *PEER Report 2003/10 Pacific Earthquake Engineering Research Center College of Engineering University of California*, Berkeley, USA, 2004.
41. Tomaževič M. Recent advances in earthquake-resistant design of masonry buildings: European perspective. *Proceedings of the 11th World Conference on Earthquake Engineering*, Acapulco, 1996; paper n. 2012.
42. Anthoine A, Magonette G, Magenes G. Shear compression testing and analysis of brick masonry walls. *Proceedings of the 10th European Conference on Earthquake Engineering*, Vienna, Austria 1994; 1657–1662.
43. NTC08 Italian Building Code. D.M. 14.01.2008: Norme Tecniche per le Costruzioni. Italian Ministry of Infrastructures and Transportation: Rome, 2008 [in Italian].
44. FEMA 306. *Evaluation of Earthquake Damaged Concrete and Masonry Wall Buildings*, Federal Emergency Management Agency, Washington, DC, USA, 1999.
45. FEMA 356. *Prestandard for the Seismic Rehabilitation of Buildings.* American Society of Civil Engineers: Reston, VA, USA, 2000.
46. Park YJ, and Ang AHS. Mechanistic Seismic Damage Model for Reinforced Concrete. *Journal of Structural Engineering ASCE* 1985; **111**(4): 722-739.
47. Petrangeli M, Pinto PE, Ciampi V. Fibre element for cyclic bending and shear of RC structures. I: Theory, *Journal of Engineering Mechanics ASCE* 1999; **125**(9): 994-1001.
48. Penna A, Lagomarsino S, Galasco A. A nonlinear macroelement model for the seismic analysis of masonry buildings. *Earthquake Engineering and Structural Dynamics* 2014; **43**(2): 159–179. doi: 10.1002/eqe.2335
49. Tortolini P, Spacone E, Petrangeli M. A RC fibre beam element for full modelling of the bending-shear response by dual section approach. *Proceedings of SSCS Numerical Modeling Strategies for Sustainable Concrete Structures*, Aix-en-Provence, France, 2012.